

Supplementary Information

Electrostatics controls the formation of amyloid-like superstructures in protein aggregation

Vito Foderà, Alessio Zaccone, Marco Lattuada, Athene M. Donald

1 Free energy of a growing aggregate.

Energy calculation

Consider the free energy of a spherical cluster with radius R with respect to the single particle forming the cluster:

$$\Delta F = -\frac{qU}{2} + \frac{3\gamma}{R} + \frac{4\pi R^3}{3} + \frac{(N \cdot n_c \cdot e)^2}{8\pi\epsilon\epsilon_0 R} - kT \cdot \log(X_N / N) \quad (1.1)$$

where q is the number of contacts between the particle in a cluster, U is the energy per contact, γ is the surface tension, R is the radius of the cluster, N the number of the particles in a cluster, n_c is the charge unit number per single particle, e is the elementary charge, ϵ and ϵ_0 are the relative dielectric constant and the permittivity in vacuum, X_N is the volume fraction of molecule in the cluster. Using the following relationships between different terms the equation can be written as a function of R :

$$q = Z \cdot N = Z \left(\frac{R}{a}\right)^{d_f}; \quad U = n_E kT;$$
$$\gamma = \frac{f \cdot U \cdot N_s}{s} = f \cdot n_E kT \frac{d_f N^{(d_f-1)/d_f}}{4\pi R^2}; \quad X_N = \frac{N (4/3)\pi a^3}{(4/3)\pi R^3} = N \frac{a^3}{R^3}$$

where Z is the number of particles neighbours, a is the radius of a single particle, f is the effective number of interactions, d_f is the fractal dimension, n_E the binding energy in kT units, s the surface of the aggregate and N_s the number of particles on the surface of an aggregate of generic fractal dimension d_f 40].

Using the above conditions, we obtain equation 2 of the main text. The so obtained equation takes into account how the change from precursor to low fractality regime affects each term of the free energy. This information is enclosed in the parameter d_f . To perform the calculations, we use the following values:

$$kT = 4.11 \cdot 10^{-21} J; \quad a = 2 \cdot 10^{-9} m; \quad \epsilon = 80; \quad \epsilon_0 = 8.854 \cdot 10^{-12} C^2 J^{-1} m^{-1} \quad e = 1.602 \cdot 10^{-19} C;$$

For $2.5 < df < 3$ we used $Z=6$ and $f =3$, for $1 < df < 2.5$ we used $Z=2$ and $f=1$. All the calculations were performed with $n_E=10$. This value for the binding energy is used to resemble the actual reversible aggregation of proteins that includes the possibility of the rearrangement of the particle within the cluster. This is in agreement with binding energies

recently estimated for aggregating ensemble of Brownian particles [41] (see also section 3 for detailed calculations). Importantly, in the specific case of aggregating proteins, the first member of the right hand side of eq. 2 in the main text refers to the binding energy between already destabilized and aggregation-prone molecules.

It is worth noting that the n_c values used in the calculations account for the average effective number of charges on a single protein. However, proteins contain polar groups that are far from being evenly distributed so that the protein surface is not uniformly charged, generating large electric dipole and multipole moments that strongly affect the inter-particle interactions [19]. Moreover, contributions due to the water structuring around the protein [20, 21], hydrophobic interactions [21] and free electrolyte mediating the interaction between proteins [22] can further contribute to the overall electrostatic interactions between two molecules. For these reasons, the electrostatic term in equation 1 represents an effective term including all the above mentioned contributions. Moreover, the fact that the dielectric properties of a protein are not constant along its length [23] means that electrostatic interactions of very different extent (i.e. with different n_c values) could take place within the same ensemble of charged proteins, determining the simultaneous occurrence of different morphologies. This is indeed experimentally verified for a number of protein systems that, in specific conditions, show the presence of both spherical and elongated aggregates [13, 27].

Our coarse-grained model considers protein molecule as hard sphere interacting via electrostatic interactions. The reason for this choice is mainly dictated by the complexity of the problem and by our goal. We tried to simultaneously keep the model at a reasonable level of simplicity, whilst not neglecting some physical properties (i.e. electrostatics, energy of binding, entropy and multi-fractal nature) that are crucial in determining the large scale arrangement of the final aggregate. Including microscopic structural features of a single molecule (i.e. secondary structure) would complicate the entire approach, whilst not providing further information in terms of large scale arrangements.

2 PBE simulations for protein aggregation: spherulites formation.

Model

The simulations of protein aggregation and spherulite formation have been performed by numerically solving population balance equations (PBEs), *i.e.*, mass balances for proteins and all of their clusters. The aggregation of proteins can be modeled as a second order kinetic process. In this case PBEs are written as follows [42, 43]:

$$\frac{dC_k}{dt} = \frac{1}{2} \sum_{i,j=1}^{i+j} K_{ij} C_i C_j - C_k \sum_{i=1}^{\infty} K_{ik} C_i, \quad (2.1)$$

where C_i is the number concentration of clusters with mass i (*i.e.*, made of i proteins), and K_{ij} is the kernel determining the rate of aggregation between two clusters, one with mass i and the other with mass j . The aggregation kernel used in the simulations is the conventional diffusion-limited kernel, which has the following form [44, 45]:

$$K_{ij} = \frac{2kT}{3\eta W_{ij}} (R_i + R_j) \left(\frac{1}{R_i} + \frac{1}{R_j} \right) \quad (2.2)$$

Where R_i is the outer radius of a cluster with mass i , W_{ij} is the stability ratio of an aggregation event between the i^{th} and j^{th} clusters, η the viscosity of water evaluated at the temperature of the experiments, k the Boltzmann constant and T the temperature.

Two types of clusters are considered in the simulations. Clusters with a radius smaller than the precursor radius R_c have a fractal dimension (d_f) equal to 3, and their radius R_i has been assumed to scale with the cluster mass as follows:

$$i = \left(\frac{R_i}{a}\right)^3 \quad (2.3)$$

where a is the protein radius. Their radius of gyration is equal to:

$$R_{g,i} = \sqrt{\frac{3}{5}} R_i \quad (2.4)$$

Clusters with a size larger than R_c have a dense precursor with a radius equal to R_c and $d_f=3$, and a shell with $d_f<3$. The radial density profile of these clusters is assumed to be continuous, switching from a constant value in the precursor to a power law in the shell:

$$\rho_i(r) = \begin{cases} \frac{3}{4\pi a^3} & 0 < r < R_c \\ \frac{3}{4\pi a^3} \left(\frac{r}{R_c}\right)^{d_f-3} & R_c < r < R_i \end{cases} \quad (2.5)$$

The outer radius of the cluster is therefore found by integrating the density over the entire cluster volume to obtain the cluster mass:

$$i = 4\pi \int_0^{R_i} \rho_i(r) r^2 dr \quad (2.6)$$

The cluster radius of gyration is analogously found from [46]:

$$R_{g,i}^2 = \frac{4\pi}{i} \int_0^{R_i} \rho_i(r) r^4 dr$$

The stability ratio W_{ij} in Equation 2.2 is computed from its definition [45]:

$$W_{ij} = 2 \int_2^{\infty} \frac{\exp\left(\frac{U_{int,ij}}{kT}\right)}{x^2} dx \quad (2.7)$$

where $U_{int,ij}$ is the interaction energy between the clusters and x is the dimensionless center-to-center distance between the clusters, normalized by the average cluster radius $(R_i+R_j)/2$. The interaction energy is the sum of two contributions: an attractive Van der Waals contribution $U_{vdw,ij}$ and a repulsive electrostatic interaction term $U_{el,ij}$:

$$U_{int,ij} = U_{vdw,ij} + U_{el,ij} \quad (2.9)$$

The Van der Waals contribution has been estimated using the well-established Hamaker equation [45]:

$$U_{vdw,ij} = -\frac{A}{6} \left(\frac{2 \cdot \mathbf{R}_i \cdot \mathbf{R}_j}{r^2 - (\mathbf{R}_i + \mathbf{R}_j)^2} + \frac{2 \cdot \mathbf{R}_i \cdot \mathbf{R}_j}{r^2 - (\mathbf{R}_i - \mathbf{R}_j)^2} + \log \left(\frac{r^2 - (\mathbf{R}_i + \mathbf{R}_j)^2}{r^2 - (\mathbf{R}_i - \mathbf{R}_j)^2} \right) \right) \quad (2.10)$$

where A is the Hamaker constant and r is the (dimensional) center-to-center distance between the two clusters. For the electrostatic repulsive energy, we have used the equation proposed by Liu and Hsu [47], which is an extension for unequal surface potential of the equations proposed by Sader et al. [48]:

$$U_{el,ij} = \frac{\pi \epsilon_0 \epsilon R_i R_j}{r} \left(\frac{kT}{e} \right)^2 \left((Y_i^2 + Y_j^2) \log \left(1 - \exp \left(-2\kappa (r - R_i - R_j) \right) \right) + 4Y_i Y_j \tanh^{-1} \left(\exp \left(-\kappa (r - R_i - R_j) \right) \right) \right) \quad (2.11)$$

where ϵ_0 is the vacuum permittivity, ϵ is water dielectric constant, κ is the reverse Debye length, e is the electron charge. The quantity Y_i is defined as:

$$Y_i = 4 \exp \left(\frac{\kappa}{2} (r - R_i - R_j) \right) \tanh^{-1} \left(\exp \left(-\frac{\kappa}{2} (r - R_i - R_j) \right) \tanh \left(\frac{e\phi_i}{4kT} \right) \right) \quad (2.12),$$

and ϕ_i is the surface potential of the i^{th} cluster.

The above equation assumes that the surface potentials of both clusters remain constant as they approach each other. In order to find the surface potential from the surface charge density, the following equation has been used [45]:

$$\frac{\sigma_i}{kT \kappa \epsilon_0 \epsilon} = 2 \sinh \left(\frac{e\phi_i}{2kT} \right) + \frac{4}{\kappa R_i} \tanh \left(\frac{e\phi_i}{4kT} \right) \quad (2.13)$$

where σ_i is the surface charge density of the i^{th} cluster.

To predict the total surface charge density on one cluster, we introduce a key physically-motivated assumption depending on whether the cluster is in the precursor regime ($d_f=3$) or possesses a multi-fractal shell. In particular, for two $d_f=3$ clusters we calculate the surface charge as the one resulting from treating the clusters as dielectric spheres. This is motivated by the compact geometry which allows us to treat compact clusters as continua. As a consequence, the surface charge density for a spherical and compact cluster is given by

$$\boldsymbol{\sigma} = \mathbf{P} \cdot \mathbf{n} \quad (2.14)$$

where \mathbf{P} is the polarization density of the body and \mathbf{n} is the unit vector normal to the surface. In a homogeneous linear and isotropic dielectric body, the polarization \mathbf{P} is aligned with and proportional to the electric field \mathbf{E} :

$$\mathbf{P} = \epsilon_0 \chi \mathbf{E},$$

where ϵ_0 is the vacuum permittivity and χ is the electric susceptibility of the body. We can integrate both sides of Eq. (2.14) over the surface of the body, and get

$$\int \sigma dS = \epsilon_0 \chi \int \mathbf{E} \cdot \mathbf{n} dS$$

We can apply Gauss' law which states that

$$\int \mathbf{E} \cdot \mathbf{n} dS = \frac{Q}{\epsilon_0}$$

where Q is the total charge of the body (i.e. sum of the charges of each single particle within the cluster). Therefore, for an isotropic distribution of charges we have $\int \sigma dS = \sigma S$, and the surface charge density is given by

$$\sigma = \chi \frac{Q}{S} = (\epsilon_r - 1) \frac{Q}{S}$$

where ϵ_r is the relative permittivity of the body. For polymers, one typically has: $\epsilon_r \sim 2-3$. Based on this, modelling our protein cluster (in the precursor regime) as a dielectric sphere, we obtain the following expression for the surface charge density for a cluster composed of N protein monomers:

$$\sigma(N) = (\epsilon_r - 1) \frac{N \times n_c e}{4\pi R^2} = (\epsilon_r - 1) \frac{N \times n_c e}{4\pi a^2 N^{2/3}} = (\epsilon_r - 1) \frac{N^{1/3} \times n_c e}{4\pi a^2} \quad (2.15)$$

Where a = monomer radius R = cluster radius $N = \left(\frac{R}{a}\right)^3$ and $n_c e$ charge per monomer.

On the other hand, for clusters in the multi-fractal regime, the aggregation involves bonding between two protruding particles on the cluster outer shell which are sufficiently isolated in space from the other particles in the clusters such that the electrostatic interactions from the other particles can be safely neglected [40, 49]. This would take into account the reduction of the electrostatic energy at decreasing d_f as predicted by equation 2 in the main text. Therefore in the aggregation rate between two clusters in the multi-fractal regime we assume that the electrostatic interaction between the two clusters reduces to the interaction between two proteins protruding from the respective outer shells. The curves reported in Figure 4a in the main text have been obtained by plotting the total energy of interaction between monomer-monomer, oligomer-oligomer (close to the critical size of the precursor), shell-monomer and shell-oligomer using equation 2.10. A very short range repulsive potential has been added to prevent overlap. According to our model, all oligomers are treated as dielectric spherical particles with a surface charge density given by equation 2.15. Instead, the interactions of aggregates with a precursor-shell structure will be controlled by monomers on their outer surface. Importantly, in the simulation all the clusters, including the precursor-shell structures, can aggregate with each other. This is to reproduce with a high degree of reliability what happens in the real system. Our kinetic model considers that, after the formation of the first precursors, the growth of the shell starts, with interactions characterized by a negligible barrier (Figure 4a in the main text). In the very early stages of the shell growth, clusters (precursor-shell) are small enough to quickly diffuse in solution and the probability for these

structures to interact with each other, is not negligible. This allows the formation of a small fraction of species with a shape that deviates from a perfect sphere (Figure S3a, left). Then, due to their increased size, further aggregation of such not perfectly spherical species with each other is extremely unlikely. However, they can still interact with oligomers and residual monomers in solution following the multi-fractal behaviour as predicted by the model. This leads to the formation of multi-fractal structures having a larger and not perfectly spherical central part (Figure S3a, right). It is worth noting that this is actually what experimentally happens. In Figure S3b we show that, even in a very small fraction, spherulites can clearly develop not only from a single spherical precursor but also from a more complex structure, being this in agreement with the prediction of our model (sketch in Figure S3a).

The numerical solution of the population balance equations has been performed by the Kumar-Ramkrishna method, as described elsewhere [44]. In a nutshell, a broad interval of cluster mass values is divided into intervals using a logarithmic spacing. The PBEs are solved for all the values of the boundaries of each interval, referred to as pivots. Each time an aggregation event leads to the production of an aggregate with mass value falling inside an interval, the aggregate is split between the two boundaries the interval. The splitting factors are selected so that two moments of the original distribution are conserved, specifically the zero and first moments. This procedure guaranties a high efficiency of the code, which allows one to simulate the evolution of a very broad cluster mass distribution.

Calculation of the multi-fractal density profile and structure factor.

To calculate the multifractal density profile (Figure 2c in the main text) the following relationship between density and d_f was used:

$$\frac{\rho(R)}{\rho_{Precursor}} = R^{[d_f(R)-3]} \quad (2.16)$$

The $d_f(R)$ was extrapolated by fitting the exponential decays after precursor formation in Figure 2b and using the fitting function within equation 2.16.

The scattering structure factor of clusters with a size smaller than R_c at a scattering vector $q=4\pi n/\lambda \sin(\theta/2)$, where n is the refractive index of the solvent, λ the wave length of the laser and θ the scattering angle, is computed assuming that they can be approximated as spheres [50]:

$$S_i(q) = \frac{9}{(qR_i)^6} (\sin(qR_i) - qR_i \cos(qR_i))^2 \quad (2.17)$$

The structure factor of precursor-shell clusters is instead computed using the Fisher-Burford equation, which is commonly used to approximate the scattering behavior of fractals [45]:

$$S_i(q) = \frac{1}{\left(1 + \frac{2}{3d_f} (qR_{g,i})^2\right)^{\frac{d_f}{2}}} \quad (2.18)$$

In the case of clusters with a multi-fractal density profile $\rho(r)$ (eq. 2.16), the scattering structure factor can be computed from the following equation [50]:

$$S_i(q) = \left(4\pi \int_0^{R_i} \rho_i(r) r^2 \frac{\sin(qr)}{qr} dr \right)^2 \quad (2.19)$$

Figure S4 shows the profile (green curve) obtained from equation 2.19. The structure factor profile for the shell growth is well approximated using a constant fractal dimension of 1.9 (black dashed line). This value was used to calculate the simulated scattering curves. This approximated structure factor is the one that has been used to calculate the time evolution of the scattering intensity (such a task would be computationally prohibitive if we were to use the actual multi-fractal form factor). Curves at $d_f=1.3$ and $d_f= 2.7$ are also shown for comparison.

Finally, the overall intensity of the scattered radiation by the entire cluster population at a scattering angle of 90° is computed through the following equation:

$$I_{90} = G \sum_{i=1}^{\infty} C_i i^2 S_i(q_{90}) \quad (2.20)$$

where q_{90} is the scattering wave vector evaluated at a scattering angle of 90° , $S_i(q)$ is the scattering structure factor of a cluster with mass i , given by Equation (2.17) for clusters with a size smaller than R_c and by Equation (2.18) for precursor-shell clusters. G is a multiplicative constant depending on the experimental scattering set up, which cannot be easily determined, and therefore the scattered intensity profile height is adjusted by fitting a few experimental data points.

3 General PBE equation includes the features of the classical nucleation theory

The complete master kinetic equation reads as:

$$\frac{dC_k}{dt} = \frac{1}{2} \sum_{i+j=k} K_{ij} C_i C_j - C_k \sum_{i=1}^{\infty} K_{ik} C_i - K_k^B C_k + \sum_{i=k+1}^{\infty} K_{ik}^B C_i \quad (3.1)$$

where the last two terms accounts for thermal breakup of a cluster of size k and generation of a k cluster by breakup of a cluster of size $k+i$. These terms are required when the inter-protein attraction is such that thermal energy can cause the complete dissociation of the bond between two proteins on a time scale comparable to the diffusive attachment time scale of a monomer. In our model the binding energy between particles is $\sim 10kT$, such that the rate of detachment of a monomer from a cluster (assuming it is bound to two particles on the surface) is according to a previous report [41], $\sim (D/\delta^2) \exp[-2 \cdot (10/kT)] \sim 2 \cdot 10^{-3} s^{-1}$, where we used the typical range of hydrophobic attraction which is of the order of 10 nm and rather independent of the chemical composition of the approaching surfaces [16, 41]. For the association rate of a monomer under diffusion-limited conditions we have $\sim (8/3)(kT/\eta)(N/V) \sim 4.8 s^{-1}$, from the standard Smoluchowski rate. Clearly, in our system the mismatch between association and dissociation rates is significant enough to neglect the last two terms in Eq. (3.1). Importantly, the absolute value that we find for the dissociation rate is such that particles certainly can rearrange during the aggregation process allowing us for setting up an equilibrium-like free energy of clustering.

However, in the general case of reactions where thermal breakup is significant, all the terms in Eq (3.1) should be considered. If we were really close to the metastability region of the proteins in water (i.e. close to the binodal line for equilibrium liquid-liquid phase separation), then a nucleation scenario within this approach can be recovered. In that case detailed balance is exactly satisfied and clusters are formed due to critical fluctuations under supersaturation conditions. Under these conditions, clusters are highly localized and noninteracting and grow very slowly by means of one-step particle attachment. Therefore, only terms of the type $K_{k-1,1}C_{k-1}$ and $K_{k,1}C_k$ contribute to the first and the second term, respectively, on the r.h.s. of Eq. (3.1). Note that we have incorporated the monomer concentration C_l in the rate constants. Under conditions of localized fluctuational growth, Eq.(3.1) in the initial stage of aggregation reduces to:

$$\frac{dC_k}{dt} = K_{k-1,1}C_{k-1} - K_{k,1}C_k - K_k^B C_k + K_{k+1,1}^B C_{k+1}$$

To shorten the notation we put $K_{k-1,1} \equiv K_{k-1}$ etc. and rewrite the equation as:

$$\frac{dC_k}{dt} = K_{k-1}C_{k-1} - K_k C_k - K_k^B C_k + K_{k+1}^B C_{k+1} \quad (3.2)$$

Since the attraction is weak and thermal dissociation is important, the principle of detailed balance is applicable in this limit. Hence, we now introduce the equilibrium or steady-state concentration of aggregates of size k as C_k^{eq} which is a Boltzmann function of the minimum work ΔF (free energy) needed to form an aggregate of size k : $C_k^{eq} \sim \exp(-\Delta F / kT)$. Upon applying the principle of detailed balance we have:

$$\begin{aligned} C_k^{eq} K_k &= C_{k+1}^{eq} K_{k+1}^B \\ C_{k-1}^{eq} K_{k-1} &= C_k^{eq} K_k^B \end{aligned} \quad (3.3)$$

These relations allow us to eliminate from Eq. (3.2) the quantities K_k^B and K_{k+1}^B , and Eq. (3.2) becomes:

$$\begin{aligned} \frac{dC_k}{dt} &= K_k \left[-C_k + C_{k+1} C_k^{eq} / C_{k+1}^{eq} \right] + K_{k-1} \left[C_{k-1} - C_k C_{k-1}^{eq} / C_k^{eq} \right] \\ &= K_k C_k^{eq} \left[C_{k+1} / C_{k+1}^{eq} - C_k / C_k^{eq} \right] - K_{k-1} C_{k-1}^{eq} \left[C_k / C_k^{eq} - C_{k-1} / C_{k-1}^{eq} \right] \end{aligned} \quad (3.4)$$

Let us now transform the discrete distribution C_k (discrete in the cluster size k) into a continuous one $C(x)$ where x is a continuous variable expressing the cluster size. Denoting by λ the spacing along the x axis between the neighbouring sizes k and $k+1$, we have $C_k = \lambda C(x)$, $C_{k+1} = \lambda C(x + \lambda)$ etc. Since λ is constant and C , C^{eq} , and K vary little within

the length λ , one can do an expansion in power series of λ and retain only the first non-vanishing term. Using this procedure, Zeldovich [51] has shown that Eq.(3.4) reduces to the following form:

$$\frac{\partial C}{\partial t} = -\frac{\partial J}{\partial x} \quad (3.5)$$

Where J is the flux in “size space” given by: $J = -D\partial C / \partial x + A \cdot C$. Here $D = \lambda K$ is the diffusion coefficient in “size space” while $A = -D \cdot \Delta F'(x) / kT$ is the drift coefficient. Therefore, our original equation can be reduced, under the assumptions stated above, to a diffusion equation (in size space) in the field of force of the free energy of aggregation. Under the circumstances that the attraction is weak in comparison with the surface energy of the cluster (i.e. the case for aggregation reactions) the free energy might go through a local maximum at a size x^* due to the competition between attraction and surface energy. Hence, clusters smaller than x^* tend to shrink whereas clusters $> x^*$ tend to grow. Then ΔF can be expanded to second order near the maximum: $F = F(x^*) - \frac{1}{2} F''(x^*)(x - x^*)^2$, and Eq. (3.5) can be solved analytically at the steady-state ($\partial C / \partial t = 0$) in the standard way of Kramers by means of the saddle-point method [52]. This yields the well-known formula of nucleation theory for the nucleation rate [53, 54]:

$$J = C_1 K_{k^*,1} \left(\frac{\Delta F''(x^*)}{2\pi kT} \right) \exp \left(-\frac{\Delta F(x^*)}{kT} \right)$$

Importantly, in the case of spherulites a process different from the standard nucleation/elongation determines the growth of the aggregates, i.e. the multi-fractal growth, and, as a consequence, no use of the rate J can be found. Finally, it is important to note that this derivation cannot be applied to earlier models because the reduction of Eq.(3.1) to Eq.(3.2) requires that one takes the interactions into account in the physical formulation of the microscopic rates K_{ij} . If the rates are taken as fitting parameters, it is impossible to recover nucleation theory.

4. Sample preparation and light scattering measurements

Bovine Insulin (BPI) was obtained as a lyophilised powder from Sigma Aldrich (I5500). Solutions at protein concentration of 4 mg/ml were prepared dissolving the powder in water with 25 mM NaCl and aliquots of 10% v/v HCl were added to the solutions to reach the desired pH value. pH measurements have an accuracy of $\text{pH} \pm 0.01$. Aggregation was thermally induced at 60°C. Details on sample preparation and light scattering measurements were previously reported [28]. Importantly, in these experimental conditions and at the end of the aggregation kinetics, native insulin molecules are mainly converted into amyloid

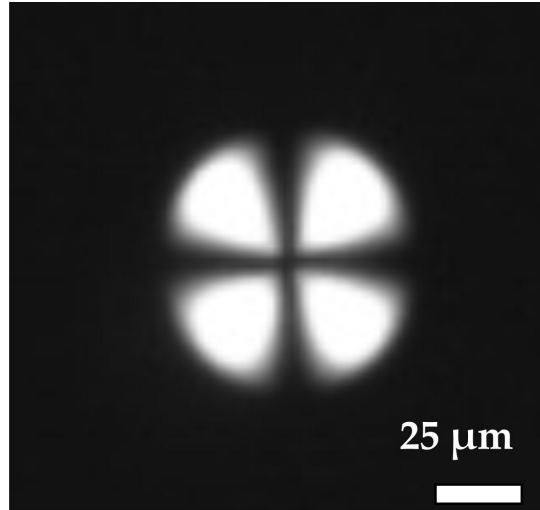
spherulites [12, 28], so that experimental data in Figure 3 are representative of spherulite growth and hence suitable for a comparison against our theoretical model.

References

- [40] A. Zaccone, D. Gentili, H. Wu, M. Morbidelli, and E. Del Gado, *Physical Review Letters* **106**, 138301 (2011).
- [41] A. Zaccone, J.J. Crassous, B. Béri, and M. Ballauff, *Physical Review Letters* **107**, 168303 (2011).
- [42] S. Kumar, and D. Ramkrishna, *Chemical Engineering Science* **51**, 1311 (1996).
- [43] D. Ramkrishna, *Population Balances: Theory and Applications to Particulate Systems in Engineering* (Academic Press 2000).
- [44] M. Lattuada, P. Sandkuhler, H. Wu, J. Sefcik, and M. Morbidelli, *Advances in Colloid and Interface Science* **103**, 33 (2003).
- [45] W.B. Russel, D.A. Saville, and W.R. Schowalter *Colloidal Dispersions* (Cambridge University Press, Cambridge 1989).
- [46] C.M. Sorensen *Aerosol Science and Technology* **35**, 648 (2001).
- [47] B.T. Liu, and J.P. Hsu, *Journal of Chemical Physics*, **130**, 044106 (2009).
- [48] J.E. Sader, S.L. Carnie, and D.Y.C. Chan, *J. Colloid Interface Sci.* **171**, 46 (1995).
- [49] T. Vicsek *Fractal Growth Phenomena* (World Scientific, Singapore 1992).
- [50] P. Lindner, and T. Zemb, *Neutron, x-ray and light scattering* (North Holland 2002).
- [51] Y.B. Zeldovich, *Acta Physicochim USSR* **18**, 1 (1943)
- [52] H.A. Kramers *Physica* **7**, 284 (1940)
- [53] J.D. Gunton, A. Shiryayev, D.L. Pagan, *Protein Condensation* (Cambridge University Press, Cambridge, p. 111, 2007).
- [54] D. Kashchiev *Nucleation. Basic Theory with Applications* (Butterworth-Heinemann, Oxford 2000).

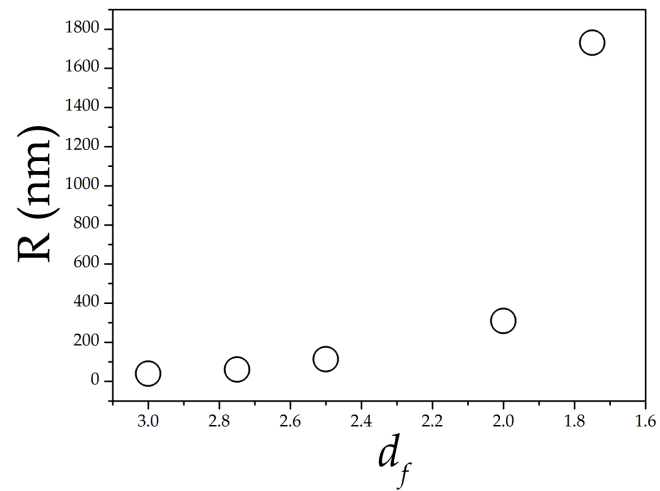
Supplementary Figures and Legends

Supplementary Figure S1



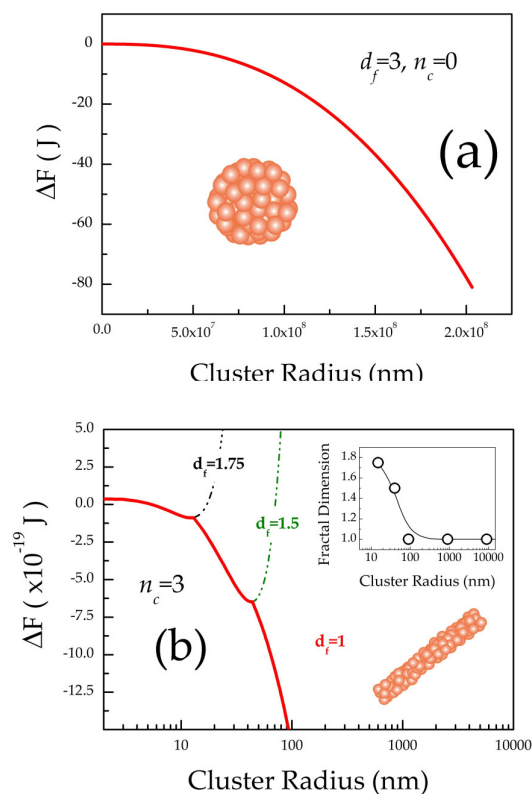
Supplementary Figure S1: Optical microscopy on amyloid spherulites. Amyloid spherulites as they appear in solution under crossed polarized optical microscope

Supplementary Figure S2



Supplementary Figure S2: Change of fractality during the growth . Radius at which the energy minima occur as a function of the fractal dimension. This shows that compact objects are formed in the early stage of the growth

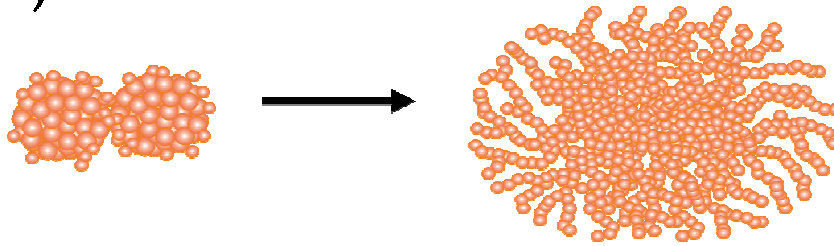
Supplementary Figure S3



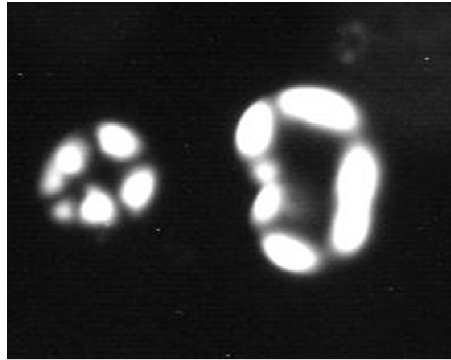
Supplementary Figure S3: Morphologies as a function of the protein charge. Free energy landscape for a growing aggregate as a function of the aggregate radius calculated by means of equation 2 (see main text) at (a) $d_f=3$ and $n_c=0$ and (b) at different fractal dimensions and with $n_c=3$. In the case of $n_c=0$, the growth proceeds with $d_f=3$ for aggregates with radii up to several cm. This means that for the range of sizes of protein aggregates experimentally observed, the growth will basically proceed as a sphere with a constant density. On the other hand, at $n_c=3$, the aggregate grows with $1 < d_f < 2$ since the very early stages of the process and then the growth proceeds with $d_f=1$ up to several cm (inset in Figure S2b). This means that a two-step process takes place: an early formation of a species with d_f slightly higher than 1 and then a linear growth of the aggregate until the reaction reaches its completion. This can resemble the classical description based on the nucleation and elongation proposed for simple elongated fibrils

Supplementary Figure S4

(a)

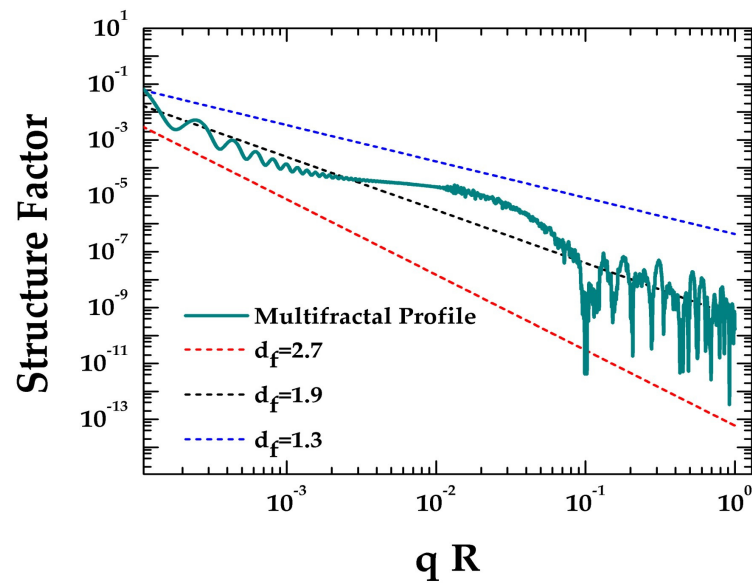


(b)



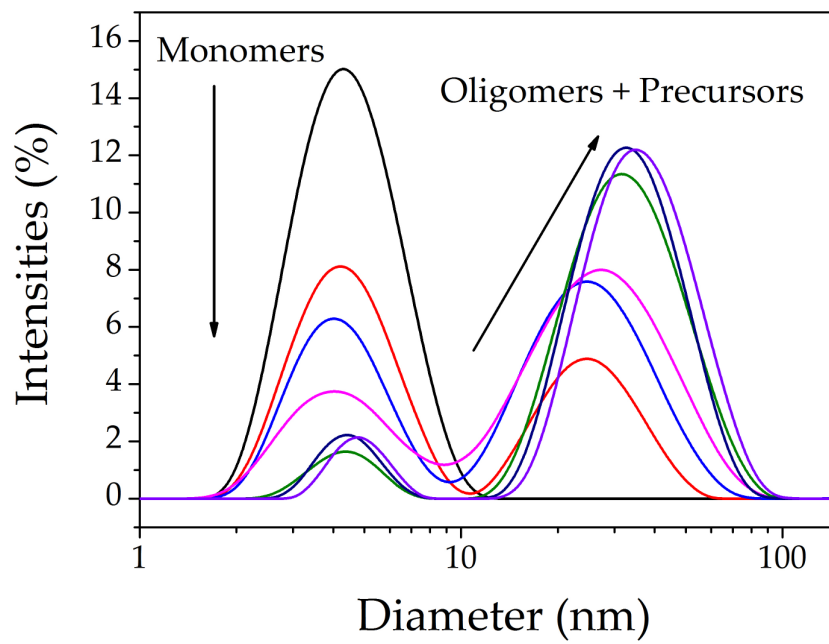
Supplementary Figure S4: Spherulites growing from complex precursor. (a) Sketch of the mechanism bringing to the formation of a small fraction of multi-fractal structures on a complex precursor. (b) Amyloid spherulites with a shell developing from a complex precursor as experimentally observed. The shell grows on two collapsed central parts.

Supplementary Figure S5



Supplementary Figure S5: Structure factor in multi-fractal regime. Structure factor as calculated from equation 2.18 (red, black and blue dashed lines) and equation 2.19 (green solid line) for fractal dimensions 2.7, 1.9, 1.3 and for the multi-fractal density, respectively.

Supplementary Figure S6



Supplementary Figure S6: Size distribution during the lag phase. Temporal evolution of the size distributions for during the lag phase of the aggregation process,

Supplementary Tab S1

pH	Effective Charge	Precursor Radius (nm)
1	0.599	31.6367
1.25	0.597	31.7491
1.5	0.582	32.6178
1.75	0.555	34.3036

Supplementary Table S1: Pairs of precursor radius and charge values used for the simulations of the spherulites kinetics as a function of the pH.